Journal of Catalysis 312 (2014) 221–231

Contents lists available at ScienceDirect

Journal of Catalysis

journal homepage: www.elsevier.com/locate/jcat

The application of inelastic neutron scattering to investigate CO hydrogenation over an iron Fischer–Tropsch synthesis catalyst

Neil G. Hamilton [a], Robbie Warringham [a], Ian P. Silverwood [a], Josef Kapitán [a], Lutz Hecht [a], Paul B. Webb [b,*], Robert P. Tooze [b], Wuzong Zhou [c], Christopher D. Frost [d], Stewart F. Parker [d], David Lennon [a,*]

[a] School of Chemistry, Joseph Black Building, University of Glasgow, Glasgow G12 8QQ, UK
[b] Sasol Technology UK Ltd, Purdie Building, North Haugh, St. Andrews, Fife KY16 9ST, UK
[c] School of Chemistry, Purdie Building, University of St. Andrews, North Haugh, St. Andrews, Fife KY16 9ST, UK
[d] ISIS Facility, Rutherford Appleton Laboratory, Chilton, Didcot, Oxon OX11 0QX, UK

ARTICLE INFO

Article history:
Received 26 November 2013
Revised 26 January 2014
Accepted 7 February 2014
Available online 13 March 2014

Keywords:
Fischer–Tropsch synthesis
Iron catalyst
CO hydrogenation
Inelastic neutron scattering

ABSTRACT

An iron Fischer–Tropsch (F–T) catalyst has been prepared and evaluated using CO hydrogenation at 623 and 723 K as a test reaction. Micro-reactor measurements establish reaction profiles. The reaction is then scaled up to enable inelastic neutron scattering (INS) measurements of the catalyst to be acquired. The INS spectra (200–4000 cm^{-1}) are characterised by a combination of hydrocarbon moieties and hydroxyl groups. Whereas the low temperature sample is characterised by an aliphatic overlayer, the hydrocarbon features of the high temperature sample are attributed to partially hydrogenated polycyclic aromatic compounds. The catalyst is further characterised by a combination of temperature-programmed oxidation, powder X-ray diffraction, Raman scattering and transmission electron microscopy. This series of measurements is combined to propose a model for the composition of the catalyst as it progresses from the precursor state to steady-state operation. The work features some of the challenges associated with using INS to characterise heterogeneously catalysed reactions systems.

1. Introduction

Fischer–Tropsch (F–T) synthesis is a well-established catalytic reaction system, using synthesis gas (CO and H_2) obtained from resources such as coal, natural gas and biomass to produce a variety of hydrocarbon products [1]. Several variants of the process operate around the world, with the catalysts predominantly based on Fe and Co containing materials [2,3]. Whereas recent large-scale unit operations have tended to feature Co catalysts [4], there is an increasing interest in Fe-based catalysts, not least as they offer the opportunity to co-synthesise olefins alongside alkanes, which otherwise tend to dominate the product slate in Fischer–Tropsch synthesis (F–TS) [5]. This new opportunity to significantly contribute to a broader base for large volume chemical feedstocks is known as the Fischer–Tropsch to Olefin (F–TO) process. Galvis and de Jong have recently comprehensively reviewed fundamental and applied aspects of the F–TO operation [6]. In order to manipulate Fe-based F–TS catalysts to favour certain product distributions, it is first necessary to understand how a standard Fe-based catalyst functions. The work outlined in this communication concentrates solely on Fe-based F–TS catalysts.

Despite wide application, there remains considerable uncertainty as to how F–TS catalysts actually operate. For example, Schulz describes 'the true F–T catalyst to be "constructed" under reaction conditions in processes of self-organisation' [7,8]. Moreover, when considering possible means for investigating the F–T process, Schulz highlights the potential of neutron scattering spectroscopy to provide new information on hydrocarbon entities likely to participate in the specific process chemistry [8]. This suggestion is insightful as the technique of inelastic neutron scattering (INS) could complement more traditional probes. For instance, analytical techniques such as Mössbauer spectroscopy, X-ray diffraction and temperature-programmed oxidation applied to Fe-based systems characterise the catalysts in terms of solid-state chemistry (haematite, magnetite and iron carbides) [9–11] and the presence of carbonaceous materials [12,13]. INS is one of the few probes that can provide information as to how hydrogen is partitioned within the catalyst matrix.

Increasingly, INS is finding application in heterogeneous catalysis. The topic has been reviewed by Albers and Parker, who have used a variety of industrially relevant examples to illustrate the

* Corresponding authors.
E-mail address: David.Lennon@glasgow.ac.uk (D. Lennon).

http://dx.doi.org/10.1016/j.jcat.2014.02.004
0021-9517/

capability of the technique [14]. Subsequently, another review by Parker and co-workers has demonstrated the further applicability of a class of neutron spectrometer previously rarely used to study adsorption phenomena and catalysis [15]. INS is ideally suited to investigate catalytic systems involving hydrogen. Due to the anomalously high neutron cross-section of ^{1}H, INS provides the means of detecting the vibrational modes of hydrogenous species over a wide spectral range (20–4000 cm^{-1}) and at reasonable resolution (10–30 cm^{-1} in favourable circumstances) [16]. Real industrial catalysts offer considerable challenges for conventional optical vibrational spectroscopy (*e.g.* infrared spectroscopy); they are often black in colour and consequently highly absorbing, possess significant metal loadings that may further absorb IR radiation, or offer a restricted spectral range due to support cut-off effects [14]. INS is not subject to these problems and can be used to acquire the hydrogen-based vibrational spectrum of a wide range of catalytic materials.

Recent work from this group has used INS to obtain the vibrational spectrum of an industrial-grade iron-based Fischer–Tropsch catalyst that had been removed from a large-scale coal-to-liquids plant [17]. Chemical extraction procedures were used to fully remove hydrocarbon product from the catalyst, so that the INS spectrum sampled material directly associated with the catalyst matrix. Ancillary TPO, elemental analysis and Raman scattering measurements showed a large pool of amorphous carbon to be present at the catalyst surface. Supplementing these measurements, a distinct INS spectrum revealed the additional presence of a hydrocarbonaceous overlayer [17]. No specific molecular species could be identified from the spectrum; however, this overlayer could be classed as comprising partially hydrogenated aromatic molecules. Further, it was speculated that this hydrocarbonaceous overlayer could play an active role in moderating the supply of reagents within the catalyst matrix during the CO dissociative adsorption and CH_x chain propagation processes [17]. Given the inherent complexity of highly formulated industrial catalysts, we decided to focus our efforts on a well-defined system in order to further investigate the role of this hydrocarbonaceous overlayer in catalysis.

Any use of INS to examine F–TS catalysts needs to delineate hydrocarbon product from hydrocarbonaceous components that may be associated with product formation. One way to minimise the complexity of the reaction system is to examine prototype F–T catalysts using the hydrogenation of CO as a test reaction. Product selectivity to CH_4 has been demonstrated to be favoured at ambient pressure on an unpromoted iron catalyst [18] and avoids the formation of long chain or heavy hydrocarbon products that would compromise subsequent INS analysis.

Whereas it is acknowledged that the ambient pressure hydrogenation of CO to CH_4 cannot be formally regarded as F–T chemistry, as no polymerisation reaction takes place, it does address aspects of Fe/CO/H_2 surface chemistry that must have connectivity to the molecular transformations associated with F–TS. The resulting knowledge base can then be applied to the more complex F–T scenario in due course. Interestingly, this study shows that CO hydrogenation over an unsupported Fe catalyst prepared in-house yields a similar INS spectrum to that reported for an industrial-grade catalyst taken from a commercial F–T reactor [17].

The paper is composed as follows. Firstly, a representative unpromoted Fe F–T catalyst is prepared and examined for CO hydrogenation using a micro-reactor arrangement at 2 representative temperatures (623 K and 723 K). Adopting a procedure recently employed to study methane reforming catalysts [19,20], the reaction is then scaled up for *ex situ* post-reaction analysis by INS. Due to the inherent insensitivity of INS, relatively large catalyst masses (10–20 g) are necessary to obtain reasonable signal-to-noise ratio spectra [21]. This requirement challenges present sample environment procedures associated with the acquisition of INS spectra of heterogeneous catalysts. The INS samples were then characterised by TPO, XRD, Raman scattering and TEM. A model of the active phase of the catalyst is proposed that includes a contribution for hydrocarbonaceous species. A probable role for this understated component of an active Fe-based catalyst is briefly considered.

Post-reaction analysis of samples from the micro-reactor and INS measurements indicate that the INS cell arrangement adopted is inefficient in reducing the catalyst. This is attributed to inferior gas/solid exchange dynamics with the INS cells, which lead to the INS samples experiencing a retarded reaction coordinate compared to the micro-reactor measurements. Despite this constraint, the INS measurements reveal new and important information; the physical differences between the INS and micro-reactor samples are discussed in terms of the evolutionary phase of the Fe/CO/H_2 reaction system [7].

2. Experimental

2.1. Catalyst preparation

The unpromoted hematite (α-Fe_2O_3) catalyst used in this investigation was prepared in-house by the precipitation technique [22]. Briefly, solutions of iron nitrate (Sigma–Aldrich $\geqslant$98%, 1 mol/L) and ammonium hydroxide (Sigma–Aldrich 28% in double-distilled H_2O, 5.6 mol/L) were co-added to a precipitating bath containing 1 L of deionised water (Elga option 3) at a rate that ensured the pH of the liquor was maintained at pH 8. A temperature of 343 K was maintained using a stirrer hot plate (IKA RCT basic with ETS-5 control). After precipitation was complete, the mixture was allowed to age at temperature for 12 h. The resultant slurry was then filtered, washed with deionised water and allowed to dry in air. The sample was then calcined at 673 K in air for a period of 8 h. The resulting solid material, dark reddish in colour, was then ground and sieved to a grain size fraction of 250–500 μm. It is this material that is used as the initial catalyst material, which is then exposed to a syngas feed at two temperatures: 623 and 723 K.

2.2. Micro-reactor measurements

Mass flow controllers (Brooks –5850) provided accurate flows of reactant gases (CO 99.5%, CK gas, H_2 99.999%, BOC) plus carrier (He 99.999%, BOC) gas. The helium line was fitted with an in-line gas filter to prevent any possible oxygen contamination (Varian Gas Clean Filter Oxygen System). All gases were fed into a mixing vessel (150 cm^3 stainless steel cylinder packed with glass Ballotini balls) which was connected via stainless steel tubing to a U-shaped tubular quartz micro-reactor (1/4″ diameter) housed within a temperature programmable furnace (Neytech 25PAF) with a thermocouple located alongside the quartz tube in order to accurately measure the temperature at the sample. The reactor was connected to the steel pipe work via Cajon compression fittings. Exit streams from the reactor were continuously monitored via an in-line quadrupole mass spectrometer (Leda Mass, Residual Gas Analyser, LM22) that sampled the elutant gas stream via a differentially pumped capillary leak fed directly into a closed ionisation source. The arrangement of the mass spectrometer was configured to confer short residence times and enhanced sensitivity.

As noted in the Introduction, the catalyst does not support F–T activity under these conditions; instead, it favours CO hydrogenation, with methane being the dominant product. Analysis of the reaction exit gas by mass spectrometry confirmed the absence of oligomeric products. Further, running the catalyst with a syngas feedstream at elevated temperatures for extended periods of time

with an in-line cold trap mounted on the outlet side of the reactor produced no detectable residues. It was therefore deduced that mass spectrometry was suitable for comprehensive analysis of the CO hydrogenation chemistry observed with this combination of feedstock and catalyst.

Reaction testing was performed using *ca.* 50 mg of the precipitated α-Fe_2O_3 precursor. Samples were treated with a 2:1 H_2/CO mixture diluted in helium (CO, 3.35 mL/min; H_2, 6.75 mL/min; He, 21.25 mL/min, total WHSV of 11.09 h^{-1}) at ambient pressure. Thus, the catalyst was activated in the presence of the reacting gases, the flows of which were maintained throughout the full reaction testing sequence. Similar conditions have been used previously to evaluate a series of prototype F–T catalysts [12]. A linear heating program of 5 K/min was applied up to the stated reaction temperature of 623 K or 723 K, where the temperature of the system was maintained for a period of 6 h. The heating program was then terminated and the catalyst sample allowed to cool to room temperature under a flow of He. CO turnover rates were based on CO consumption at pseudo steady-state conditions compared to the CO MS signal before reaction. Before removal from the micro-reactor, passivation of reacted samples was achieved using a standard procedure where the concentration of oxygen that the sample is exposed to is gradually increased up to atmospheric levels [2].

2.3. Inelastic neutron scattering measurements

INS measurements of surface species present on heterogeneous catalysts require relatively large sample sizes (10–20 g) as a consequence of the inherent insensitivity of the INS technique. To accommodate this high degree of scale-up, a relatively high capacity reactor arrangement was used, the set up of which is described elsewhere [21]. Approximately 25 g of the fresh catalyst was weighed into a large quartz reactor (3/4″ diameter) contained within a bucket furnace (Instron SFL, model no. TF105/3/12/F controlled by a Eurotherm model 3508 temperature controller). The furnace was packed with quartz wool to minimise thermal gradients. Dilution of the catalyst bed to reduce potential thermal gradients was not possible, as it would lead to reduced signal: noise spectra and could potentially compromise spectral resolution. Reactions were carried out using a 2:1 H_2/CO mixture diluted in He (CO, 75 mL/min; H_2, 150 mL/min; He, 775 mL/min; total WHSV of 0.53 h^{-1}) at ambient pressure and subjected to a linear heating program of 5 K/min up to the stated reaction temperature of either 623 K or 723 K. It is acknowledged that the large volume reactor was operated at a lower space velocity than that attainable with the micro-reactor. This was a consequence of limitations within the scale-up procedure, not least the volumes and flows of CO and H_2 that could be accommodated within the experimental hall of the neutron facility. The mass spectrometer of the INS gas handling apparatus was not calibrated for reactant or product gases and therefore no quantitative conversion data are available. Nevertheless, despite these issues, comparable reaction profiles were observed from the micro-reactor and the INS reactor, indicating that similar chemistry was being explored in both cases. After a period of 6 h at the stated reaction temperature, the catalyst was allowed to cool to room temperature under a flow of the He. The reactor was then purged with helium to remove residual gaseous species before being isolated and transferred to an Argon filled glovebox (MBraun UniLab MB-20-G, $[H_2O] < 1$ ppm, $[O_2] < 2$ ppm). Within the inert atmosphere of the glove box, the sample was loaded into aluminium sachets that were then secured via indium seals within a standard aluminium INS cell [16]. Care was taken to position the sachets inside the cell such that the entire catalyst sample was contained within the neutron beam path. This arrangement means that the spectrum corresponds to the whole sample and sensitivity constraints preclude spectral acquisition from particular zones within the reactor, *i.e.* it was not possible to discern whether the catalyst close to the gas inlet had a different composition to material close to the reactor outlet. In this way, the INS spectrum represents an average of the full catalyst charge.

INS spectra were recorded using the MAPS direct geometry neutron spectrometer located at the ISIS Facility [15]. INS spectra were recorded with incident neutron energies of 4840 cm^{-1} and 2017 cm^{-1}. These incident neutron energies provide good spectral resolution over the 200–4000 cm^{-1} spectral range [20].

Recent work from this group has demonstrated how INS can be used to provide quantitative information on hydrogenous moieties present at the surface of industrial-grade metal catalysts [23]. Following this approach, the integrated intensity of the ν(CH) and ν(OH) bands of each of the catalyst samples after syngas exposure was determined by fitting the data to a single Gaussian function using the Origin graphical software package (MicroCal Origin, Version 6.1). The areas were then compared to calibration curves obtained previously for the MAPS spectrometer [23], enabling the quantity of hydrogen associated with carbon and oxygen atoms retained at the catalyst surface to be determined.

2.4. Catalyst characterisation

2.4.1. Pre-reaction

Before reaction testing, catalyst samples were characterised using N_2 physisorption, powder X-ray diffraction (XRD) and Raman spectroscopy. N_2 physisorption measurements were performed using a Micromeritics Gemini 2370 instrument. XRD measurements were performed on a Siemens D5000 powder diffractometer using Cu Kα radiation in Bragg-Brentano geometry in the 2θ range 5–110° (step size 0.02°, 10 s/step) using approximately 1 g of ground sample. Raman characterisation used a custom instrument [24] utilising backscattering geometry and a 532 nm source at <20 mW power. Higher laser powers were observed to damage the sample. A holographic transmission grating and a back-thinned CCD detector were employed for data collection. Catalyst samples were ground with KBr in an approximately 15:1 ratio and the self-supporting discs were held in the laser focus. Data were collected for approximately two minutes, with removal of cosmic rays carried out in the control software.

2.4.2. Post-reaction

After reaction testing in the micro-reactor arrangement, samples were characterised *ex situ* by XRD and TEM. XRD measurements were recorded using a Panalytical X'Pert Pro X-ray diffractometer with Co K$\alpha_{1,2}$ radiation from 10° to 90° (2θ), scan rate 1.34°/min, at ambient temperature. Quantitative phase analysis to determine the relative amounts of the crystalline phases was undertaken using Rietveld techniques as part of Panalytical's X'Pert HighScore Plus software. TEM and high-resolution TEM (HRTEM) characterisation of micro-reactor samples was performed on a JEOL JEM-2011 electron microscope operated at 200 kV, equipped with an Oxford Link ISIS energy dispersive X-ray spectroscopy (EDX) system and a Gatan 794 camera. The powder specimens were deposited on a copper grid with a holey carbon film, and the images were recorded on some particles above holes to avoid a noisy background of amorphous carbon.

As described in Section 2.3, reaction measurements were scaled up to accommodate measurements by INS. After INS analysis, the reacted samples were analysed *ex situ* by elemental analysis, temperature-programmed oxidation (TPO), XRD, Raman scattering and TEM. The INS gas handling apparatus was unable to perform the standard passivation procedure post-reaction, so a different passivation procedure had to be adopted. After INS acquisition, the samples were retained in the Al INS measurement cells and left

in a storage cupboard for several (⩾5) days under ambient conditions. A slow ingress of air over time led to passivated samples. Before XRD and Raman measurements, samples were ground so as to avoid sample inhomogeneity which may arise during the scaled-up reaction. Repeat measurements were also performed to ensure reproducibility with these measurements. Elemental analysis, performed using an Exeter Analytical C440 Elemental Analyser, was unable to detect the presence of hydrogen in the post-reaction sample. Thus, the detection limit for hydrogen for this instrument, ⩽0.3 wt%, sets an upper limit for the extent of retained hydrogen. Raman scattering measurements were undertaken using a Horiba Jobin Yvon LabRam HR800 microscope fitted with a 50× LWD objective. An excitation wavelength of 514 nm was used. Spectra were collected with varying laser intensities and collection times to prevent laser damage of the sample. Typically, 1% or 10% neutral density filters were used to reduce a laser power of between 2 and 5 mW. Several spots were analysed from each sample to ensure uniformity of measurement. TPO measurements utilised the same reactor arrangement described in Section 2.2. Approximately 50 mg of reacted catalyst sample was loaded into the previously described sample environment and a diluted O_2 gas flow (5% O_2/He, BOC, 50 mL/min) was passed over the sample whilst being subjected to a linear temperature ramp of 10 K/min up to 1200 K. The eluting gases were sampled via in-line quadrupole mass spectrometry. Detection and quantification of the oxidation of carbon species contained within each sample was achieved by monitoring the CO_2 signal (m/z 44). Quantification of the evolved CO_2 was achieved by calibration procedures using TPO measurements of graphite (Sigma–Aldrich, >99.5%), and thermal decomposition measurements of calcium carbonate (BDH, 98%) [20].

The microstructure of the scaled up and reacted INS catalyst samples was studied by transmission electron microscopy (TEM) using a Tecnai T20 microscope with an accelerating voltage of 200 keV. Samples were dispersed in methanol before being deposited on holey carbon film (300 μm mesh grid, Agar scientific) prior to inspection. The possibility of changes to the carbon structure and distribution on the cooling of sample post-reaction, as discussed by Janboroers and co-workers in their *in situ* TEM studies on the carburisation process of iron-based F–TS catalysts [25] was not factored in to the analysis of the *ex situ* TEM images.

3. Results and discussion

3.1. Catalyst characterisation

Nitrogen physisorption of the catalyst indicated a total surface area of 32.1 $m^2\,g^{-1}$. The XRD diffractogram (Supplementary Data, Fig. S1) is assigned to α-Fe_2O_3 (hematite) [26]. Raman analysis of the sample (Supplementary Data, Fig. S2) further indicates the iron oxide phase to be hematite [27]. A broad Raman band centred at ~1700 cm^{-1}, reported elsewhere [17], is attributed to a matrix effect of KBr that is used as a diluent for spectral acquisition.

3.2. Micro-reactor studies

3.2.1. Reaction testing at 623 K

The reaction profile for CO hydrogenation over the α-Fe_2O_3 starting material at 623 K is presented in Fig. 1(a). The profile presented in Fig. 1(a) is characterised by two main CO_2 features (420 K and 605 K), two H_2O features (465 K and 620 K) and a single CH_4 feature (605 K). Simultaneously, CO and H_2 are observed to be consumed with CO uptake greater than that of H_2. The production of CO_2 and H_2O between 420 K and 465 K could be the result of the stepwise reduction of the α-Fe_2O_3 starting material towards Fe^0 via Fe_3O_4 and FeO by CO and H_2 resulting in the evolution of CO_2 and H_2O respectively [28]. Several contributing pathways could

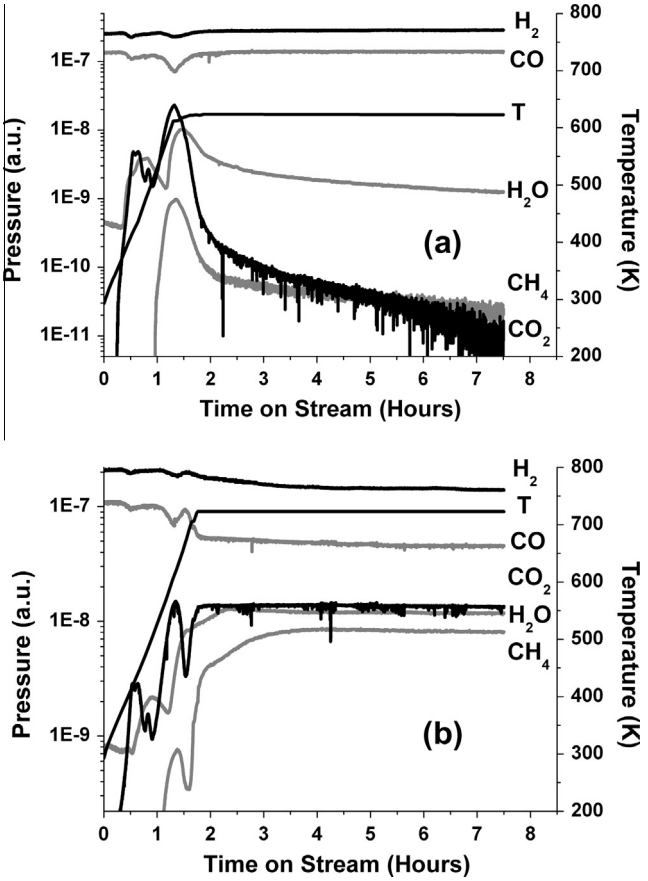

Fig. 1. Profile for the reaction of CO and H_2 (1:2) over precipitated α-Fe_2O_3 at (a) 623 K and (b) 723 K. The mass traces are labelled in descending order at the right side of the profile.

be responsible for the second CO_2 feature at 605 K. Firstly, CO in the presence of metallic iron will carbidise the catalyst via CO disproportionation (Boudouard reaction) [29,30] and/or CO dissociation [29,30]. Carbon deposition by these routes would explain the increase in CO_2 signal and also the increase in CH_4 signal, with a higher concentration of surface carbon available for hydrogenation to form CH_4. CO_2 production as a result of CO oxidation with surface oxygen could also occur. The increase in H_2O signal at 623 K could be attributed to the hydrogenation of surface oxygen after CO dissociation. The water–gas-shift (WGS) reaction [31] could also be active in consuming CO at 623 K to form CO_2 and H_2. Iglesia et al have previously discussed pathways for oxygen removal via reaction with adsorbed hydrogen and through WGS activity on an Fe–Zn F–T catalyst [32] and found the reaction between adsorbed oxygen and hydrogen was the preferred pathway for water formation. After approximately 2 h on stream, the CO_2 and CH_4 signals decrease accompanied by a slower decrease in the H_2O signal. Within this regime, CO conversion is approximated at <1%. Adopting the methodology of Galvis and co-workers [33], the catalytic activity approximates to an iron time yield (FTY) of 0.7×10^{-5} mol CO $g_{Fe}^{-1}\,s^{-1}$, similar to values reported by Galvis et al. under comparable reaction conditions [33].

Initial analysis of Fig. 1(a) would suggest that a temperature of 623 K is insufficient to sustain CO hydrogenation over this sample. However, it is recognised that under actual F–TS conditions, catalytic performance may decrease during the first hours on stream but then increase with increasing time-on-stream [34]. Therefore, although Fig. 1(a) would suggest that catalytic activity cannot be sustained, the authors acknowledge that on increasing reaction time, the catalyst could attain a respectable level of activity.

3.2.2. Reaction testing at 723 K

The reaction profile for the hydrogenation of carbon monoxide at 723 K is presented in Fig. 1(b). Within the first 1.7 h, *i.e.* up to 623 K, the features of the reaction profile are comparable to those observed in Fig. 1(a). After 1.8 h, there is an increase in the CO_2, H_2O and CH_4 signals and the catalyst approaches a steady-state regime after 3 h on stream. CO conversion under these pseudo steady-state conditions is approximately 42% with the catalytic activity approximating to a FTY of 0.305 mmol CO g_{Fe}^{-1} s^{-1}. This FTY value exceeds that recently reported by Galvis et al. for F–TS over iron-based catalysts but that work was conducted at a reduced temperature of 623 K [33]. Fig. 1(b) shows CO_2 and CH_4 production to follow similar profiles, with CO_2 assuming steady-state production more rapidly. The stabilised CH_4 and CO_2 yields at higher temperature for $t > 3$ h indicates that the methanation reaction and the WGS reaction are active at this stage of the reaction coordinate. At this pseudo steady state, the production of CH_4, CO_2 and H_2O may be described by the following four elementary reactions.

$$C_{(ad)} + 4H_{(ad)} \rightarrow CH_{4(g)} \quad (1)$$

$$CO_{(g)} + O_{(ad)} \rightarrow CO_{2(g)} \quad (2)$$

$$CO_{(g)} + H_2O_{(g)} \rightarrow CO_{2(g)} + H_{2(g)} \quad (3)$$

$$O_{(ad)} + 2H_{(ad)} \rightarrow H_2O_{(g)} \quad (4)$$

3.3. Post-reaction characterisation of micro-reactor samples

Preliminary characterisation of the reacted 623 K and 723 K samples was performed using XRD and TEM. The overlaid XRD patterns are presented in Fig. 2 and indicate that the crystalline composition of the reacted samples to be very similar irrespective of the reaction temperature. Both samples show the presence of iron carbides, the composition of which was determined by Rietveld refinement to be predominately Hägg carbide (χ Fe_5C_2) with cementite (Fe_3C) also present [35]. Details of the Rietveld analysis are presented in the Supplementary Data (Figs. S3 and S4). As the diffractograms presented in Fig. 2 are almost identical, it is suggested that the formation of iron carbides proceeds regardless of the reaction temperature, even though catalytic activity varies greatly (Fig. 1(a) and (b)). No graphitic features were observed in the XRD measurements.

TEM of the 623 K and 723 K samples are presented in Figs. 3 and 4 respectively, with micrographs of the enlarged areas provided in Figs. S5 and S6 of the Supplementary Data. The 623 K sample

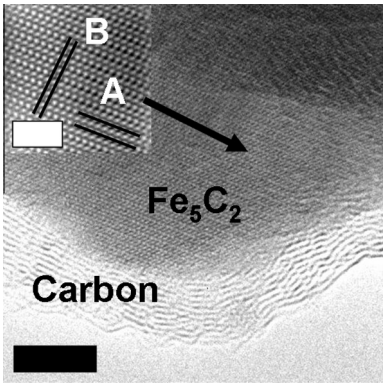

Fig. 3. HRTEM of 623 K reacted sample with the inset FFT image and enlargement of the indicated area. The *d*-spacing marked by **A** is 0.492 nm, that by **B** is 0.285 nm and the angle between them is 84.7°. These are characteristic of monoclinic Fe_5C_2. The white scale bar represents 2 nm and the black bar represents 5 nm.

(Fig. 3) is characterised by a polycrystalline carbon shell of an approximate thickness of 3–4 nm. The insert of Fig. 3 shows a high-resolution image of the particle's core. The lattice spacing at **A** is 0.492 nm ($d(001) = 0.501$ nm) and at **B** is 0.285 nm ($d(310) = 0.293$ nm), with the angle between **A** and **B** being 84.7°. These figures compare well with those expected for monoclinic Fe_5C_2: $d(001) = 0.501$ nm, $d(310) = 0.293$ nm and $\angle d(001)$, $d(310) = 84.1°$. In some of the micrographs collected, small iron oxide crystallites were observed buried within the outer carbon shell (not shown). Indexing of the *d*-spacing indicates these iron oxide species to be tetragonal Fe_2O_3 ($a = 0.834$ nm, $c = 0.8322$ nm); however, this species is not present in the corresponding sample diffractogram (Fig. 2). A possible explanation for this is that the iron oxide crystallites are too small for detection by XRD. The 723 K sample micrograph (Fig. 4) offers a similar compositional make up to the 623 K sample with an iron carbide core of monoclinic Fe_5C_2 as determined from *d*-spacing measurements (not shown). However, there is a reduction in the polycrystalline carbon outer layer, with an increased presence of tetragonal Fe_2O_3 surrounding the carbidic core as indicated by the *d*-spacing in Fig. 4, which matches well with the unit cell of tetragonal Fe_2O_3, with **A** indicating a spacing of 0.267 nm (cf $d(301) = 0.264$ nm) and **B** indicating a spacing of 0.277 nm (cf $d(212) = 0.278$ nm), the angle between **A** and **B** being 64.1° (cf $\angle d(301)$, $d(212) = 65.2°$). The carbonaceous overlayer observed in Fig. 3 is thought to be responsible for the lack of activity apparent in Fig. 1(a). The eventual outcome of carbon within this

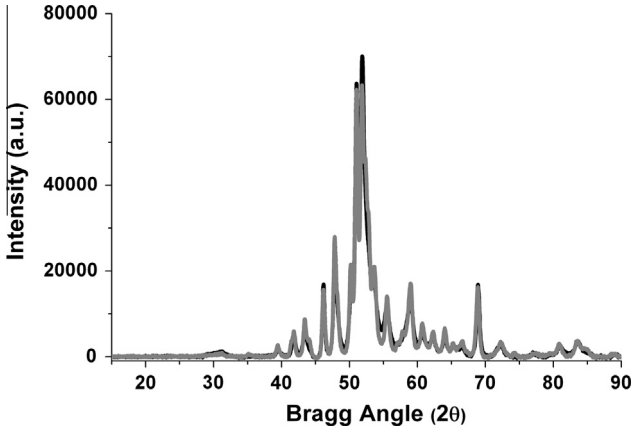

Fig. 2. XRD pattern for post-reaction micro-reactor samples of the Fe catalyst after exposure to a CO/H_2 mixture (1:2) at 623 K (black line) and 723 K (grey line).

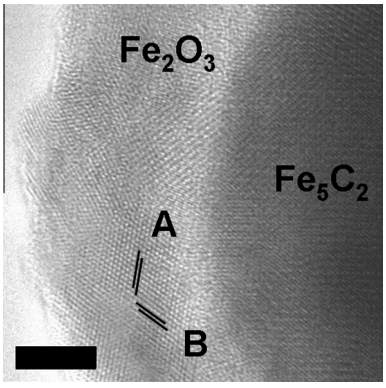

Fig. 4. HRTEM of 723 K reacted sample. The *d*-spacing marked by **A** is 0.267 nm, the *d*-spacing marked by **B** is 0.277 nm, these are characteristic of tetragonal Fe_2O_3. The black bar represents 5 nm.

reaction system can be surmised within Niemantsverdriet's competition model [11], where different competing pathways for the formation of carbon products, (*i.e.* iron carbide, polymeric carbon or reaction product) occur. Thus, the availability of adsorbed hydrogen relative to adsorbed carbon influences the outcome of the retained carbon; with hydrogen supply at 723 K being sufficient to sustain methane production over the reaction time studied (Fig. 1(b)).

3.4. Inelastic neutron scattering measurements

The INS spectra recorded at 4840 cm^{-1} for the reacted samples are presented in Fig. 5, with 5(a) presenting the spectrum of the fresh catalyst and 5(b) and 5(c) presenting the 623 and 723 K data sets, respectively. The weak neutron scattering intensity evident in Fig. 5(b) and (c) is indicative of a relatively low concentration of hydrogen within both reacted catalyst matrices. This is consistent with the elemental analysis measurements (Section 2.4.2), which could not detect the presence of hydrogen. The detection limits of this instrument ($\leqslant$0.3 wt%) therefore set an upper limit on the hydrogen content of these samples. However, it is noted that the intensity significantly exceeds that previously seen with nickel methane catalysts [20], indicating a relatively greater degree of hydrogen retention with the Fe-catalysed reactions considered here.

The spectrum of the fresh catalyst (Fig. 5(a)) has a single broad feature centred at 3442 cm^{-1}. This feature could arise from two sources. Firstly, it is possible that the in-house catalyst contains a small presence of goethite (α-FeOOH) due to incomplete calcination during the catalyst preparation stage. However, X-ray diffraction (Fig. 2) shows no evidence for this species so, if it is present, it is to a small degree. Alternatively, the 3442 cm^{-1} band could reflect a population of hydroxyl groups present as surface terminations of the hematite (α-Fe_2O_3) precursor compound.

The 623 K sample has two principle bands at 3640 and 2955 cm^{-1}, with the former assigned to terminal surface hydroxyl groups. The band centred at 2955 cm^{-1} is attributed to the ν(CH) mode of deposited hydrocarbonaceous material and indicates the presence of sp^3 hybridised carbon atoms.

The spectrum of the 723 K sample (Fig. 5(c)) displays 3 peaks that are centred at 3621, 3385 and 3060 cm^{-1}. The features located at 3385 cm^{-1} and 3621 cm^{-1} are respectively assigned to ν(OH) stretching modes of bridging and terminal hydroxyl groups that are thought to derive from H_2O formation during the catalyst reduction from α-Fe_2O_3. The peak at 3060 cm^{-1} is assigned to ν(CH) modes of retained hydrocarbons, with a marked shift to higher wavenumber and a stronger intensity relative to that seen in the 623 K sample (Fig. 5(b)), indicating an increased contribution from sp^2 hybridised carbon atoms, *i.e.* olefinic and/or aromatic hydrocarbons. This deduction is consistent with the work of Loaiza-Gil and co-workers who report the presence of aliphatic or polyaromatic species remaining adsorbed on the surface of iron catalysts active for the hydrogenation of CO hydrogenation [36].

The INS spectra recorded at an incident energy of 2017 cm^{-1} are presented in Fig. 6. Fig. 6(a) presents the fresh catalyst and is principally defined by a sharp feature centred at 806 cm^{-1} that disappears on reaction (Fig. 6(b) and (c)). This band could possibly be an out-of-plane OH deformation either attributed to a hydroxyl phase of iron oxide, *i.e.* goethite, or a terminal surface hydroxyl group of α-Fe_2O_3. Previous INS studies performed on bulk goethite show in-plane and out-of-plane hydroxyl deformations of approximately equal intensity at ~1000 and ~880 cm^{-1} respectively [37,38]. The absence of a 1000 cm^{-1} band from Fig. 6(a) would suggest that the 806 cm^{-1} peak is not associated with goethite. Furthermore, the XRD diffractogram of the fresh catalyst (Fig. S1) shows the iron oxide phase to be uniquely α-Fe_2O_3. The 806 cm^{-1} feature is therefore assigned to a magnon feature of α-Fe_2O_3 [39,40]. Neutrons possess nuclear spin, making the detection of magnetic features such as magnons possible [16]. This assignment requires further investigation.

Fig. 6(a) shows the presence of a substantial population of hydroxyl groups and these must have bending modes. There are broad features at ~950 and ~320 cm^{-1} which we assign to the in-plane and out-of plane deformation modes of a terminal hydroxyl on α-Fe_2O_3. A broad band at ~600 cm^{-1} is present in Fig. 6(a)–(c). We assign this to Fe–O stretch modes in agreement with previous work [38,41]. Although neither Fe nor O has any significant incoherent cross-section, INS samples all of the material; thus, the large number of Fe–O modes present in the bulk results in an observable feature. As both α-Fe_2O_3 and Fe_3O_4 have FeO_6 octahedra in their structures, only minor differences in the transition energy would be expected, exactly as found.

Fig. 6(b) represents the 623 K data set and is characterised by bands at 1478, 951, 607 and 310 cm^{-1}. The 1478 cm^{-1} band is assigned to a C–H deformation. With reference to the aliphatic ν(CH) counterpart in Fig. 5(b), this is tentatively linked to a CH_2 scissors mode of an alkane [41]. The relatively sharp peak at 951 cm^{-1} is assigned to an OH in-plane deformation mode of the hydroxyl groups encountered in Fig. 5(b). The broad band centred at 607 cm^{-1} is attributed to a combination of A_{1g} Fe–O phonon modes

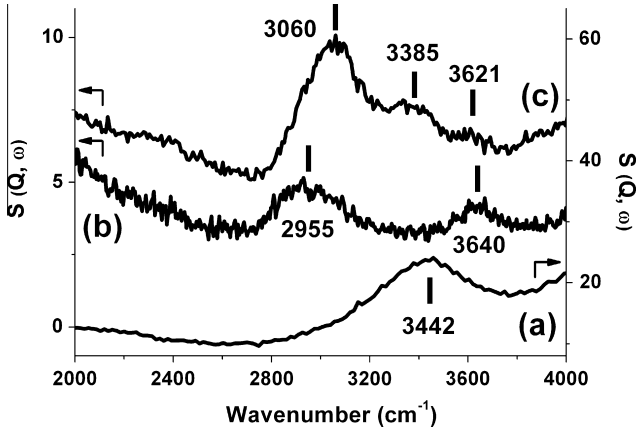

Fig. 5. INS spectra of (a) precursor α-Fe_2O_3 and post-reaction samples after reaction with CO/H_2 mixtures (1:2) at (b) 623 K and (c) 723 K. Spectra were recorded at an incident energy of 4840 cm^{-1}.

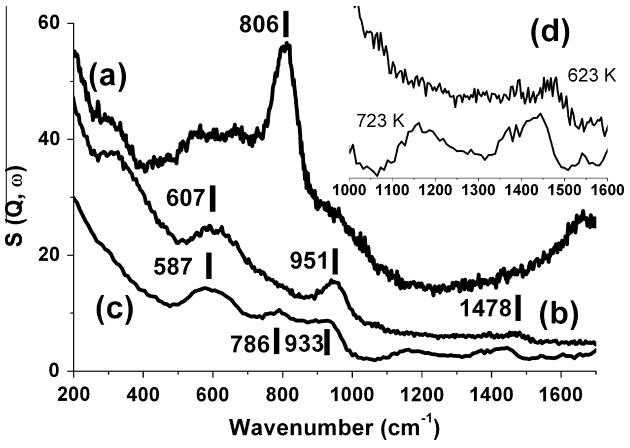

Fig. 6. INS spectra of the (a) precursor α-Fe_2O_3 and post-reaction samples after reaction with CO/H_2 mixtures (1:2) at (b) 623 K and (c) 723 K. The inset spectrum (d) is an enlargement of the 623 K (top) and 723 K (bottom) spectra between 1000 and 1600 cm^{-1}. Spectra were recorded at an incident energy of 2016 cm^{-1}.

associated with a Fe_3O_4 (magnetite) component of the catalyst [42]. The peak at 310 cm^{-1} could represent further iron-derived phonon modes and/or an out-of-plane OH deformation mode. The weakness and relatively simple nature of the spectrum, (aliphatic C–H stretch and CH_2 scissors), argues for a low concentration of aliphatic species. The high energy of the O–H stretch at 3640 cm^{-1}, which is close to that found for free hydroxyls on oxide surfaces, indicates that there is little or no interaction between the hydrocarbonaceous adlayer and the hydroxyls.

The INS spectrum for the 723 K sample recorded at a primary energy of 2017 cm^{-1} is more complex than that of the 623 K spectrum and is presented in Fig. 6(c), with bands at 1542, 1447, 1380, 1160, 933, 786, 587 and 184 cm^{-1}. The signals at 1447 cm^{-1} and 1542 cm^{-1} have been a source of some controversy in the literature [41,43,44]. However, following work from Albers et al. [45], they are tentatively assigned to semi-circle ring deformation modes, possibly coupled with a δ(CH) mode that is associated with perimeter carbons of an extended polycyclic aromatic network. The 1380 cm^{-1} feature conforms to an in-plane ring deformation of a naphthalene type molecule [46]. The 1160 cm^{-1} feature can be attributed to an in-plane CH deformation, whereas the 786 cm^{-1} band corresponds to an out-of-plane CH wag. The inset in Fig. 6 presents an enlargement of the low and high temperature samples in the 1000–1600 cm^{-1} region (Fig. 6(d)), where the absence of the in-plane CH deformation at 1160 cm^{-1} is evident in the low-temperature spectrum. In a similar fashion to its low temperature counterpart, the 933 cm^{-1} feature is assigned to an OH in-plane deformation mode of hydroxyl groups.

The spectra shown in Figs. 5 and 6 show a marked change in the nature of the adlayers obtained for reaction at 623 and 723 K. Whereas that formed at 623 K is largely aliphatic, at 723 K it is largely aromatic. Further, the layer may be interacting with the hydroxyls as shown by the downshifted O–H stretch at 3385 cm^{-1}. Overall, the high temperature spectrum (Figs. 5(c) and 6(c)) is similar to that found for hydrocarbonaceous overlayers formed at comparable temperatures [19,20].

Figs. 5(c) and 6(c) define the vibrational spectrum of an iron-based catalyst that is able to sustain methane production over the 6-h time period. Alkyl groups containing multiple $-[CH_2]_n-$ moieties couple in-phase giving rise to intense and predictable INS signals typically located at *ca.* 720 cm^{-1} and 1300 cm^{-1}, respectively, assigned to CH_2 rock and CH_2 twist deformations [17]. No such intense signals are observed in any of the spectra presented here, supporting the proposal that the hydrocarbonaceous component on this iron catalyst after exposure to syngas at 723 K can be defined by an extended polycyclic aromatic hydrocarbonaceous residue, exhibiting some aliphatic character, with minimal contribution from linear alkanes. Unfortunately, the spectra are not sufficiently distinct to enable a precise molecular assignment for the species that correlate with sustained methane production (Fig. 1(b)). Nevertheless, it is noted that considering differences between the MAPS neutron spectrometer used in this work and the TOSCA neutron spectrometer used to study the industrial F–T iron-based catalyst discussed in the Introduction [17], the hydrocarbonaceous species present in both cases are broadly comparable. This is an important outcome and establishes the relevance of using the CO hydrogenation reaction to probe the surface chemistry connected with iron-based F–T catalysts.

3.5. Powder X-ray diffraction measurements

A comparison of the *ex situ* powder XRD diffractograms for both samples post-INS analysis is presented in Fig 7. The diffractogram of the sample reacted at 623 K is presented in Fig 7(a) and indicates the sample to be composed primarily of Fe_3O_4 [47]. This is different from the micro-reactor sample presented in Fig. 2, where the XRD

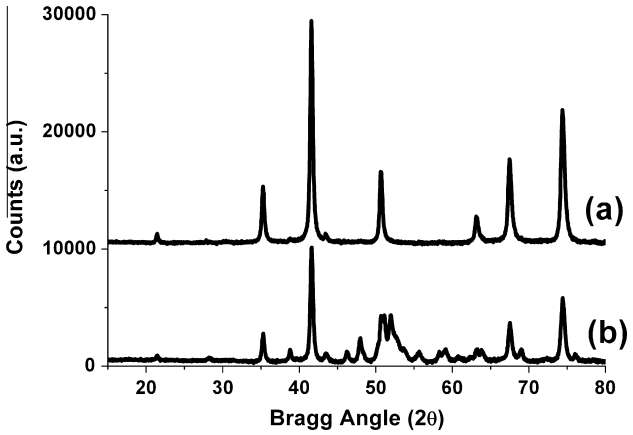

Fig. 7. XRD pattern for post-reaction samples of the Fe catalyst after exposure to a CO/H_2 mixture (1:2) at (a) 623 K, and (b) 723 K.

is composed almost entirely of iron carbide. The XRD diffractogram of the 723 K sample (Fig 7(b)) indicates the catalyst to exist in a more reduced state than the 623 K sample, with iron carbide reflections between the range of 50–55° more prominent in the diffractogram. The composition of the sample as determined using Rietveld analysis indicates the sample to be composed of approximately 50:50 magnetite to iron carbide (see Supplementary Data, Fig. S7). These XRD measurements indicate that the INS catalyst samples have not been fully reduced during the reaction testing. This has occurred due to restrictions in the gas exchange characteristics of the large volume INS cells. This issue will be considered further in Section 4. Future work will address these challenging INS sample environment issues. Nevertheless, the INS spectra in Figs. 5 and 6 show important aspects of the $Fe/CO/H_2$ surface chemistry. It is noted that a small reflection at 21.5° is present in both Fig. 7(a) and (b), which could be attributed to graphitic carbon [12]. However, the lack of intensity of this sharp feature in relation to the remainder of the diffractogram would suggest that this feature is more likely a minor reflection attributed to Fe_3O_4 rather than graphitic carbon, which usually exhibits a broader profile.

3.6. Raman spectroscopy

The Raman spectrum was recorded for the catalyst sample treated in syngas at 623 K (not shown) and at 723 K (Fig. 8). Both spectra are similar and dominated by carbon-carbon stretching features at 1340 cm^{-1} and 1603 cm^{-1}. A small band located at 664 cm^{-1}

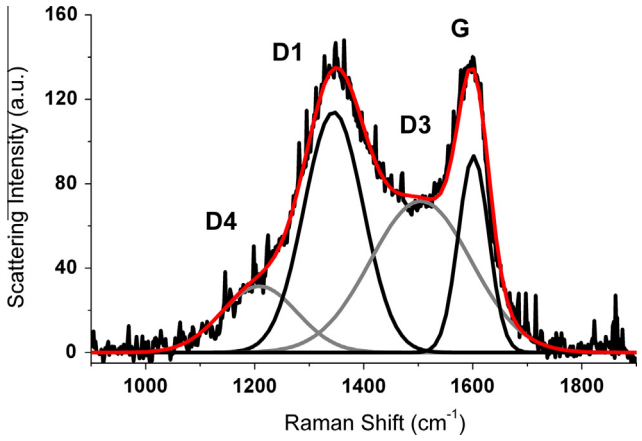

Fig. 8. Raman spectrum for post-reaction samples of the Fe catalyst after exposure to a CO/H_2 mixture (1:2) at 723 K. Peak assignment from left to right: D4, D1, D3, G.

(not shown) is assigned to the E_u mode associated with the magnetite component of the sample [27]. The 'G' band located at 1604 cm^{-1} is attributed to the E_{2g} mode of ordered sp^2 hybridised carbon atoms [48,49]. The 'D' band at 1334 cm^{-1} is assigned to the A_{1g} mode of disordered carbon [50]. It is possible to further analyse the 'D' peak of the Raman spectrum into a series of sub-peaks: a D1 band located at 1340 cm^{-1} originates from a double resonant Raman scattering process consisting of a defect and an in-plane transverse optic phonon mode in a graphene lattice; a D2 band at ~1620 cm^{-1} is ascribed to E_{2g} symmetry of surface graphene layers; a D3 band at ~1500 cm^{-1} is attributed to amorphous carbon; and a D4 band at ~1200 cm^{-1} represents A_{1g} symmetry within the disordered graphitic lattice [48,50,51]. The fitting presented in Fig. 8 does not include the D2 band, as it was not possible to ascertain with confidence the presence of this feature. Given that no graphite was detectable by XRD (Fig. 7), the Raman spectrum in Fig. 8 is assigned to an amorphous carbonaceous overlayer.

3.7. Transmission electron microscopy

TEM microscopy of the reacted catalyst samples is presented in Figs. 9 and 10. The 623 K catalyst (Fig. 9) is characterised by a series of particles of apparently random size and shape. Some particles are coated with a distinct overlayer of thickness *ca.* 5 nm (as indicated by the black arrow in Fig. 9) that is attributed to the amorphous carbon indicated in the Raman spectrum (Fig. 8). The bulk of the material is attributed to Fe_3O_4 as indicated by the XRD pattern (Fig. 7(a)). Fig. 10(a) presents a low magnification TEM image for the 723 K sample and shows this catalyst to be composed of a series of dense, elliptical inclusions surrounded by an outer layer. These ellipses are superimposed upon an abundant, less dense material, also assumed to be carbon. Fig. 10(b) shows a high-magnification image of one of the particles with the inset of Fig. 10(b) present an enlargement of the area indicated by the black arrow. The outer layer seen previously in Fig. 10(a) can be estimated in Fig. 10(b) to be *ca.* 5 nm thick. The lattice fringes observed in the figure inset of Fig. 10(b) have a *d*-spacing of 0.209 nm, which is consistent with it being iron carbide or Fe_3O_4 [9,52]. Fig. 10(a) resembles micrographs reported by Shroff and co-workers, who also examined the reaction of syngas over bulk iron catalysts [9].

3.8. Quantitative analysis using INS and temperature-programmed oxidation

A major advantage of INS is that the signal intensity associated with a specific mode is directly proportional to the number of hydrogen atoms participating in that particular oscillation [15,23]. Thus, by adopting calibration procedures outlined in Ref. [23], the spectral intensity of the INS spectra presented in Figs. 5 and 6 can be quantified.

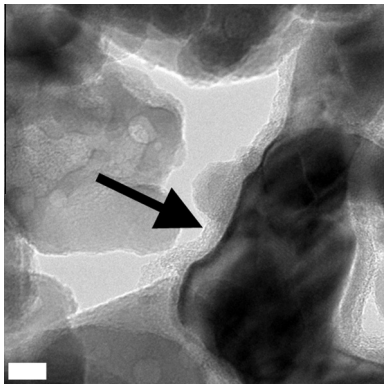

Fig. 9. HRTEM of 623 K reacted sample after analysis by INS with the black arrow indicating the thick carbon outer layer. The white scale bar represents 10 nm.

The ν(CH) band of the 623 K sample (Fig. 5(b)) corresponds to a hydrogen content of 296 ± 18 μmoles H $g^{-1}_{(cat)}$ (0.0298% w/w), with the error representing one standard deviation in triplicate INS measurements for hydrogen content of a standard sample [23]. Increasing the reaction temperature to 723 K increases the intensity of this band (Fig. 5(c)), yielding a hydrogen content of 755 ± 47 μmoles H $g^{-1}_{(cat)}$ (0.0761% w/w). Integration of the terminal hydroxyl band, $\nu(OH)_t$, corresponds to a hydrogen content for the 623 K and 723 K samples of 93.6 ± 6 μmoles H $g^{-1}_{(cat)}$ (0.0094% w/w) and 80.1 ± 5 μmoles H $g^{-1}_{(cat)}$ (0.0081% w/w) respectively. The band for bridging hydroxyl groups, $\nu(OH)_b$, is only present for the 723 K spectrum (Fig. 5(c)) and corresponds to a hydrogen content of 338 ± 21 μmoles H $g^{-1}_{(cat)}$ (0.0341% w/w). These values are presented in Table 1.

Ex situ TPO measurements were performed in order to evaluate and quantify the carbon present on the catalyst post-reaction. The TPO profile for the 623 K sample (Fig. 11(a)) is characterised by T_{max} at 630 and 670 K. The integrated response of the CO_2 signal corresponds to 158 ± 12 μmoles C $g^{-1}_{(cat)}$ (0.190% w/w, Table 1). The 723 K sample is noticeably more intense and is characterised by a broad feature, T_{max} = 720 K, that includes low temperature inflections at 580, 610 and 660 K (Fig. 11(b)). The asymmetry of this feature suggests that several carbonaceous species are contributing to the desorption feature. Quantification of the CO_2 peak area indicates a carbon content of 6167 ± 479 μmoles C $g^{-1}_{(cat)}$ (7.40% w/w, Table 1), a quantity 39 times greater than the 623 K sample. With reference to the XRD, Raman and TEM measurements, carbon from the 723 K sample is thought to predominantly originate from a combination of amorphous carbon and iron carbide. Table 1 shows that carbon associated with hydrogen atoms, that gives rise to the INS spectra seen in Figs. 5 and 6, will make a marginal contribution to the desorption profile shown in Fig. 11(b).

4. Discussion

Linking the INS and TPO measurements together enables a C:H ratio for the two catalysts to be determined; C:H values of 1:1.88 and 1:0.12 apply to the low and high temperature samples respectively, Table 1. It is informative to consider candidate molecules that could be present in the case of the high temperature sample that exhibits sustained methane yields. The INS spectra of the 723 K reacted sample (Figs. 5(c) and 6(c)) are indicative of an overlayer of partially hydrogenated polyaromatic hydrocarbons (Section 3.4). Candidate molecules could therefore be partially hydrogenated anthracene or partially hydrogenated naphthalene, which yield C:H ratios between 1:1.25 and 1:1.4. The C:H ratio for the 723 K sample is so hydrogen deficient that such candidate molecules cannot account for the general trend. In fact, a C:H ratio of 1:0.12 is so skewed towards carbon that it prompts alternative explanations. The vibrational spectrum for the high temperature catalyst defined by Figs. 5(c) and 6(c) more closely resembles a heterogeneous distribution of molecular species rather than hydrogen decorating edge atoms of amorphous carbon. For instance, the INS profile in the 800–1200 cm^{-1} region of amorphous carbon [45] differs from that observed in Fig 6(c). This suggests that a small population of hydrocarbonaceous moieties, displaying a definable molecular footprint, *i.e.* partially hydrogenated polyaromatic hydrocarbons, co-exist with a larger population of amorphous carbon, that is additionally supplemented by the presence of iron carbides. This scenario defines the components of an iron-based F–T catalyst that is active for CO hydrogenation over a 6-h reaction period. Conventional sample analysis, *e.g.* XRD, TEM, Raman, etc., is

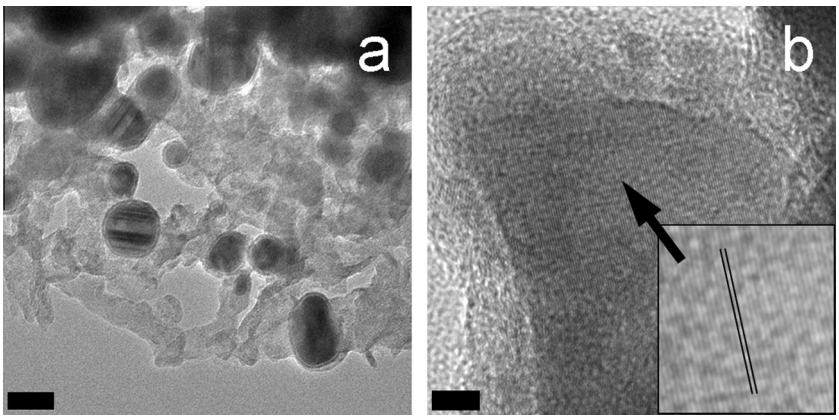

Fig. 10. HRTEM of 723 K reacted sample after analysis by INS. The inset in part b is an enlargement of the indicated area, with the *d*-spacing as indicated by the black lines presenting 0.209 nm. The black scale bar represents (a) 50 nm and (b) 2 nm.

Table 1
Quantification of hydrocarbonaceous features retained by the catalyst after 6 h on stream at 623 and 723 K. Hydrogen associated with carbon and oxygen atoms has been determined from the integrated intensity of ν(CH) and ν(OH) features in the INS spectra (Fig. 5). The hydroxyl population can be sub-divided into bridging [$\nu(OH)_b$] and terminal [$\nu(OH)_t$] hydroxyl groups. The carbon retention value is obtained from TPO measurement (Fig. 11). The C:H ratios are derived from the carbon TPO values and the hydrocarbon INS features (ν(CH)).

Reaction Temperature K	INS ν(CH) $\left(\mu mol\ H\ g^{-1}_{(cat)}\right)$	INS $\nu(OH)_b$ $\left(\mu mol\ H\ g^{-1}_{(cat)}\right)$	INS $\nu(OH)_t$ $\left(\mu mol\ H\ g^{-1}_{(cat)}\right)$	TPO Carbon retention $\left(mmol\ C\ g^{-1}_{(cat)}\right)$	C:H
623	296 ± 18	–	93.6 ± 6	0.158 ± 0.012	1:1.88
723	755 ± 47	338 ± 21	80.1 ± 5	6.17 ± 0.479	1:0.12

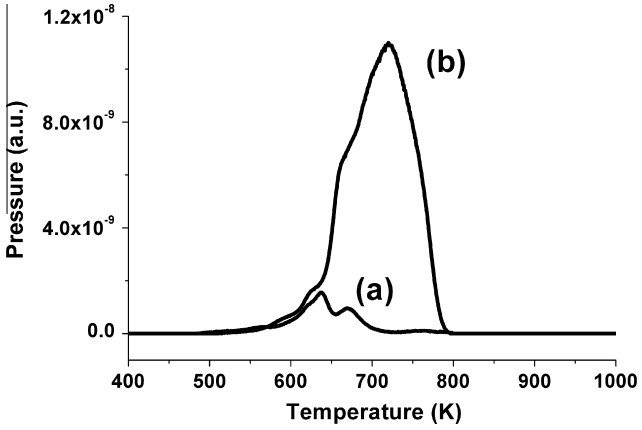

Fig. 11. Comparison of post-reaction temperature-programmed oxidation profiles for the Fe catalyst exposed to a CO/H_2 mixture (1:2) at (a) 623 K and (b) 723 K.

unable to detect the presence of a discrete hydrocarbonaceous overlayer. INS has uniquely been able to define this component of the catalytic system.

The C:H ratio for the low temperature sample is also carbon rich compared to candidate aliphatic species indicated by the INS spectra (Figs. 5(b) and 6(b)). Thus, a similar co-existence of carbonaceous entities existing alongside a small population of hydrocarbonaceous species (aliphatic) is envisaged for this sample as well.

Section 3.3 establishes that CO hydrogenation at 723 K over a self-prepared Fe catalyst leads to broadly comparable hydrocarbonaceous species to that reported for a commercial F–TS catalyst extracted from a large-scale C–T–L F–T reactor [17]. This then prompts one to consider a probable role for the overlayer in the F–T process. Clearly, the CO hydrogenation reaction requires dissociative adsorption of both CO and H_2. With reference to XRD measurements (Figs. 2 and 7(b)) and literature reports [9,12], an iron carbide surface is a reasonable candidate for inducing the dissociation and subsequent hydrogenation steps that lead to the CH_4 formation observed in Fig. 1(b). Thus, it is at the iron carbide surface where carbon and hydrogen uniquely combine. Assuming this to be correct, it then seems reasonable to further surmise that this spatial domain is where a hydrocarbonaceous overlayer resides. From the information presented in this work, it is not possible to determine whether the hydrocarbonaceous overlayer is a "spectator" species [53] or an active component of a working F–TS catalyst. That important question is beyond the scope of the present work but, nevertheless, it does appear that the INS spectrum can be associated with an operational phase of Fe-based catalysts active in CO/H_2 chemical transformations.

Contained within the wealth of F–T literature are a number of insightful graphics that schematically illustrate the key stages as a Fe precursor compound, invariably α-Fe_2O_3, is transformed into a working F–TS catalyst [9,54–56]. The work presented here allows us to consider an additional component in these graphical representations; namely a hydrocarbonaceous overlayer at the surface of the active iron carbide phase, Fig. 12. Fig. 7(b) shows the presence of magnetite, indicating that the reaction conditions experienced within the INS sample cell (reduced space velocity compared to the more conventional micro-reactor measurements) have meant that the hematite precursor is only partially reduced and Fig. 12 seeks to define the extent of reduction as referred to the INS measurements. Future work will address limitations of the INS sample environment. Fig. 12 can be sub-divided into three stages: Stage I represents the α-Fe_2O_3 precursor compound; Stage II represents the inter-conversion of α-Fe_2O_3 to Fe_3O_4 that is accompanied by the formation of iron carbide; and Stage III represents the different chemical compositions depending on starting temperature.

At 623 K, the composition is defined as predominately Fe_3O_4, with a presence of iron carbide and an associated hydrocarbonaceous aliphatic overlayer. An outer layer of amorphous carbon is present surrounding the Fe_3O_4 core. However, for the 723 K sample

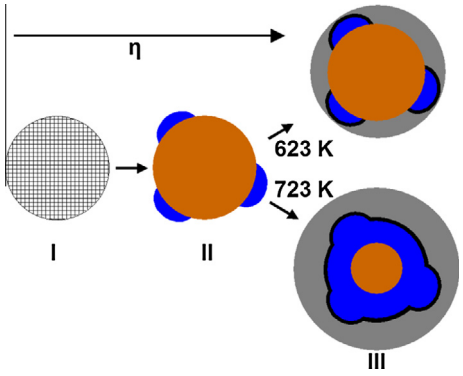

Fig. 12. Schematic representation of restructuring of α-Fe_2O_3 precursor in the INS experiments on continuing exposure to a CO/H_2 mixture (1:2) at elevated temperature. The reaction coordinate, η, increases from left to right of the figure. The colour scheme is as follows; chequered – α-Fe_2O_3, orange – Fe_3O_4, blue – iron carbide, black – hydrocarbonaceous overlayer, grey – amorphous carbon. Roman numerals indicate the three stages of the catalysts conditioning process, as discussed in the text (Section 4). The hydrocarbonaceous overlayer is aliphatic in the sample reacted at 623 K, whereas it is assigned to partially hydrogenated polyaromatic molecules in the case of the 723 K sample. (For interpretation of the colour references in this figure legend, the reader is referred to the web version of this article.)

the composition can be thought of being at a more advanced stage of the reaction coordinate than that seen for the 623 K sample. Thus, the extent of Fe_3O_4 has diminished with an expansion of an iron carbide phase, plus the formation of a partially hydrogenated aromatic hydrocarbonaceous overlayer as evidenced in Figs. 5(c) and 6(c). There is a greater retention of amorphous carbon under these conditions, as signified by the larger outer layer surrounding the core. Both branches of Stage III of Fig. 12 account for the partial reduced state of the catalyst that is a consequence of the constrained gas exchange characteristics of the INS reaction cell.

The physical differences between the post-reaction characterisation measurements of micro-reactor and INS catalyst samples, *e.g.* XRD (Figs. 2 and 7), may be rationalised within Schultz's concept of an evolutionary process [7], with the INS sample profile somewhat retarded with respect to that achievable in the micro-reactor. It is presumed that with extended time-on-stream the INS catalyst samples would eventually exhibit complete conversion to iron carbide, much as the micro-reactor catalyst samples have achieved. And, as mentioned in Section 3.2.1, with reference to the work of Pérez-Alonso and co-workers [34], it is also possible that CO hydrogenation activity could be sustained at 623 K for extended times on stream. A lack of temporal coincidence between the reaction coordinate for the two sets of cells (micro-reactor and INS cells) has not compromised the value of the new information uniquely accessible by INS. The INS measurements are invaluable in showing that formation of a hydrocarbonaceous overlayer occurs for both the low and high temperature sample treatments. A heightened understanding of how different reduction profiles affect the form of the vibrational spectrum of this overlayer, and how that correlates to CO hydrogenation activity constitutes 'work in progress'.

5. Conclusions

A bulk iron oxide F–TS catalyst has been prepared and characterised. Micro-reactor measurements examining the hydrogenation of CO have established reaction profiles for this material at 623 and 723 K. The reaction was then scaled up, so that INS spectra of the two catalyst samples post-reaction could be acquired. The INS samples were further characterised by a combination of XRD, Raman scattering, TEM and TPO. The main results may be summarised as follows.

- Over a 6-h period, the Fe-based catalyst can sustain methanation activity at 723 K but not at 623 K.
- The INS spectrum of the catalyst sample operated at 623 K is assigned to an inhomogeneous population of aliphatic molecules.
- The INS spectrum of the catalyst sample operated at 723 K is assigned to an inhomogeneous population of partially hydrogenated polyaromatic molecules. The spectrum exhibits comparable characteristics to that reported for an industrial-grade catalyst operated in a commercial F–TS reactor.
- Analysis of the INS spectra of the low and high temperature samples determines the extent of hydrogen atoms bound to carbon atoms at the catalyst surface to be respectively 296 ± 47 and 755 ± 47 μmoles H $g^{-1}_{(cat)}$.
- A schematic diagram for the transition of precursor compound to active catalyst is proposed, which includes the presence of a hydrocarbonaceous overlayer as an integral component of the working catalyst matrix.
- Post-reaction characterisation shows that there is a marked difference between the active catalyst's composition when used for the micro-reactor studies and the INS measurements despite the precursor being identical. In both cases, the catalyst is active for methanation. The larger sample size and lower space velocity of the INS reaction cell results in incomplete conversion to iron carbide. This outcome is thought to reflect aspects of the "construction phase" [7] associated with this particular catalytic system.

Acknowledgments

Sasol Technology UK Ltd., STFC (CCLRC) and the University of Glasgow are thanked for the provision of studentships (NGH and RW). The development of INS sample cells and associated sample handling capability was supported by funding from the EPSRC (Grant Number EP/E028861/1). The STFC Rutherford Appleton Laboratory is thanked for access to neutron beam facilities. Mr. Mark Kibble and Mr. Chris Goodway (ISIS Facility, STFC Rutherford Appleton Laboratory) are acknowledged for their assistance in commissioning the INS reaction system. Technical assistance in electron microscopy was provided by Mr. Jim Gallagher and Mr. Colin How (University of Glasgow).

Appendix A. Supplementary material

Supplementary data associated with this article can be found, in the online version, at http://dx.doi.org/10.1016/j.jcat.2014.02.004.

References

[1] A.P. Steynberg, Stud. Surf. Sci. Catal. 152 (2004) 1.
[2] M.E. Dry, Appl. Catal., A 138 (1996) 319.
[3] D. Leckel, Energy Fuels 23 (2009) 2342.
[4] M.E. Dry, Stud. Surf. Sci. Catal. 152 (2004) 533.
[5] H.M.T. Galvis, J.H. Bitter, C.B. Khare, M. Ruitenbeek, A.I. Dugulan, K.P. de Jong, Science 335 (2012) 835.
[6] H.M.T. Galvis, K.P. de Jong, ACS Catal. 3 (2013) 2130.
[7] H. Schulz, Top. Catal. 26 (2003) 1.
[8] M. Claeys, R. Cowan, H. Schulz, Top. Catal. 26 (2003) 139.
[9] M.D. Shroff, D.S. Kalakkad, K.E. Coulter, S.D. Kohler, M.S. Harington, N.B. Jackson, A.G. Sault, A.K. Datye, J. Catal. 156 (1995) 185.
[10] J.W. Niemantsverdriet, A.M. van der Kraan, J. Catal. 72 (1981) 385.
[11] J.W. Niemantsverdriet, A.M. van der Kraan, W.L. van Dijk, H.S. ven der Baan, J. Phys. Chem. 84 (1980) 3363.
[12] T. Herranz, S. Rojas, F.J. Pérez-Alonso, M. Ojeda, P. Terreros, J.L.G. Fierro, J. Catal. 243 (2006) 199.

[13] R.A. Dictor, A.T. Bell, J. Catal. 97 (1986) 121.
[14] P.W. Albers, S.F. Parker, Adv. Catal. 51 (2007) 99.
[15] S.F. Parker, D. Lennon, P.W. Albers, Appl. Spectrosc. 65 (2011) 1325.
[16] P.C.H. Mitchell, S.F. Parker, A.J. Ramirez-Cuesta, J. Tomkinson, Vibrational Spectroscopy using Neutrons. Series on Neutron Techniques and Applications, World Scientific, Singapore, 2005.
[17] N.G. Hamilton, I.P. Silverwood, R. Warringham, J. Kapitán, L. Hecht, P.B. Webb, R.P. Tooze, S.F. Parker, D. Lennon, Angew. Chem., Int. Ed. 52 (2013) 5608.
[18] B. Graf, H. Schulte, M. Muhler, J. Catal. 276 (2010) 66.
[19] I.P. Silverwood, N.G. Hamilton, A.R. McFarlane, J. Kapitán, L. Hecht, E.L. Norris, R.M. Ormerod, C.D. Frost, S.F. Parker, D. Lennon, Phys. Chem. Chem. Phys. 14 (2012) 15214.
[20] A.R. McFarlane, I.P. Silverwood, R. Warringham, E.L. Norris, R.M. Ormerod, C.D. Frost, S.F. Parker, D. Lennon, RSC Adv. 3 (2013) 16577.
[21] I.P. Silverwood, N.G. Hamilton, A. McFarlane, R.M. Ormerod, T. Guidi, J. Bones, M.P. Dudman, C.M. Goodway, M. Kibble, S.F. Parker, D. Lennon, Rev. Sci. Instrum. 82 (2011) 034101.
[22] F.J. Pérez-Alonso, M.L. Granados, M. Ojeda, P. Terreros, S. Rojas, T. Herranz, J.L.G. Fierro, M. Gracia, J.R. Gancedo, Chem. Mater. 17 (2005) 2329.
[23] I.P. Silverwood, N.G. Hamilton, C.J. Laycock, J.Z. Staniforth, R.M. Ormerod, C.D. Frost, S.F. Parker, D. Lennon, Phys. Chem. Chem. Phys. 12 (2010) 3102.
[24] L.D. Barron, E.W. Blanch, I.H. McColl, C.D. Syme, L. Hecht, K. Nielsen, Spectroscopy 17 (2003) 101.
[25] S. Janbroers, P.A. Crozier, H.W. Zandbergen, P.J. Kooyman, Appl. Catal., B: Environ. 102 (2011) 521.
[26] Joint Committee on Powder Diffraction Standard Card #13–534.
[27] D.L.A. de Faria, S. Venâncio Silva, M.T. de Oliveira, J. Raman Spectrosc. 28 (1997) 873.
[28] A.J.H.M. Kock, H.M. Fortuin, J.W. Geus, J. Catal. 96 (1985) 261.
[29] A. Kadkhodayan, A. Brenner, J. Catal. 117 (1989) 311.
[30] E. Kawasaki, J. Sanscrainte, T.J. Walsh, AIChE 8 (1962) 48.
[31] M.E. Dry, ChemTech 12 (1982) 744.
[32] S. Krishnamoorthy, A. Li, E. Iglesia, Catal. Lett. 80 (2002) 77.
[33] H.M.T. Galvis, J.H. Bitter, T. Davidan, M. Ruitenbeek, A.I. Dugulan, K.P. de Jong, J. Am. Chem. Soc. 134 (2012) 16207.
[34] F.J. Pérez-Alonso, T. Herranz, S. Rojas, M. Ojeda, M. López Granados, P. Terreros, J.L.G. Fierro, M. Gracia, J.R. Gancedo, Green Chem. 9 (2007) 663.
[35] J.J. Retief, Powder Diffr. 14 (1999) 130.
[36] A. Loaiza-Gil, B. Fontalb, F. Ruedac, J. Mendialduac, R. Casanova, Appl. Catal., A: Gen. 177 (1999) 193.
[37] P.C.H. Mitchell, J. Tomkinson, Catal. Today 9 (1991) 227.
[38] P.G. Hall, N.S. Clarke, S.C.P. Maynard, J. Phys. Chem. 99 (1995) 5666.
[39] E.J. Samuelsen, G. Shirane, Phys. Status Solidi 42 (1970) 241.
[40] S.N. Klausen, K. Lefmann, P.A. Lindgård, K.N. Clausen, M.F. Hansen, F. Bødker, S. Mørup, M. Telling, J. Magn. Magn. Mater. 266 (2003) 68.
[41] I. Chamritski, G. Burns, J. Phys. Chem. B 109 (2005) 4965.
[42] D. Lin-Vien, N.B. Colthup, W.G. Fateley, J.G. Graselli, The Handbook of Infrared and Raman Characteristic Frequencies of Organic Molecules, Academic Press, Boston, 1991.
[43] H.D. Babcock, L.L. Herzberg, Astrophys. J. 108 (1948) 167.
[44] L.V. Gasparov, D.B. Tanner, D.B. Romero, H. Berger, G. Margaritondo, L. Forró, Phys. Rev. B: Condens. Matter Mater. Phys. 62 (2000) 7939.
[45] P.W. Albers, J. Pietsch, J. Krauter, S.F. Parker, Phys. Chem. Chem. Phys. 5 (2003) 1941.
[46] T. Fukushima, H. Arakawa, M. Ichikawa, J. Chem. Soc., Chem. Commun. 11 (1985) 729.
[47] Joint Committee on Powder Diffraction Standard Card #19-629.
[48] M.A. Pimenta, G. Dresselhaus, M.S. Dresselhaus, L.G. Cancado, A. Jorio, R. Saito, Phys. Chem. Chem. Phys. 9 (2007) 1276.
[49] R.J. Nemanich, S.A. Solin, Phys. Rev. B 20 (1979) 392.
[50] A. Sadezky, H. Muckenhuber, H. Grothe, R. Niessner, U. Pöschl, Carbon 43 (2005) 1731.
[51] J. McGregor, Z. Huang, E.P.J. Parrott, J.A. Zeitler, K.L. Nguyen, J.M. Rawson, A. Carley, T.W. Hansen, J.-P. Tessonnier, D.S. Su, D. Teschner, E.M. Vass, A. Knop-Gericke, R. Schlögl, L.F. Gladden, J. Catal. 269 (2010) 329.
[52] P. Moodley, F.J.E. Scheijen, J.W. Niemantsverdriet, P.C. Thüne, Catal. Today 154 (2010) 142.
[53] P.S. Cremer, X.C. Su, Y.R. Shen, G.A. Somorjai, J. Am. Chem. Soc. 118 (1996) 2942.
[54] M.E. Dry, Catal. Lett. 7 (1990) 241.
[55] M. Ding, Y. Yang, B. Wu, T. Wang, L. Ma, H. Xiang, Y. Li, J. Mol. Catal. A: Chem. 351 (2011) 165.
[56] F. Gao, H. Wang, M. Qing, Y. Yang, Y. Li, Chin. J. Catal. 34 (2013) 1312.